Systematic characterization of maturation time of fluorescent proteins in living cells

Enrique Balleza, J Mark Kim & Philippe Cluzel

The slow maturation time of fluorescent proteins (FPs) limits the temporal accuracy of measurements of rapid processes such as gene expression dynamics and effectively reduces fluorescence signal in growing cells. We used high-precision time-lapse microscopy to characterize the maturation kinetics of 50 FPs that span the visible spectrum at two different temperatures in *Escherichia coli* cells. We identified fast-maturing FPs from this set that yielded the highest signal-to-noise ratio and temporal resolution in individual growing cells.

FPs are commonly used to monitor dynamic cellular processes in a wide variety of biological systems. Nascent FPs, however, must undergo a stochastic maturation step to become fluorescent; the kinetics of this maturation process directly affect the accuracy with which biological processes can be monitored. While many studies have exhaustively compiled *in vitro* characteristics of FPs[1–4], the maturation times of FPs in living cells remain sparsely characterized[5,6], and no single 'gold-standard' method has been established for carrying out such measurements. The lack of systematic maturation measurements might be due to the inherent complexity of the maturation process, which involves, in addition to the folding of the β-barrel, torsional rearrangements, cyclization, oxidation and dehydration of the chromophore[7]. However, even if the full details of these processes are not completely understood, a systematic empirical characterization of maturation times of FPs in living cells would be highly valuable, as it would help researchers select the fastest maturing proteins or be aware of artifacts inherent to slow FPs.

To measure maturation kinetics with high precision, we used an agarose-based, single-cell chemostat that allowed us to image and track hundreds of bacterial colonies growing exponentially in a tightly regulated environment for more than 30 generations[8] (**Supplementary Fig. 1**). This setup also allowed us to precisely control the delivery of chloramphenicol, a translation inhibitor widely used to assess maturation times[6,9], via microfluidic flow. When cells producing FPs are exposed to this drug, translation is rapidly arrested, but FP maturation continues. As previously synthesized proteins mature and become visible, the fluorescence signal continues to increase despite the absence of newly synthesized FPs (**Supplementary Figs. 2–4**). From the fluorescence increase, we quantified the fraction of immature protein at the time of translation arrest and extracted the kinetics of maturation (**Supplementary Fig. 5**). We effectively eliminated photobleaching from our measurements by reducing exposure time to the lowest possible values (**Supplementary Note**).

FP maturation is often modeled as a first-order process with single exponential kinetics and a characteristic half-time (t_{50}). However, we observed highly diverse maturation kinetics (see **Supplementary Note** for all maturation curves), even for FPs that form the same chromophore. Some variants, such as mEGFP, exhibited simple first-order kinetics—the fraction of immature protein as a function of time followed a single exponential (**Fig. 1a**). The maturation of other variants, such as mGFPmut2, however, was better described by two exponentials indicating the existence of effectively two kinetic steps in the maturation process (**Fig. 1b**). In a third example, the maturation rate of wild-type GFP (wtGFP) was initially slow but progressively became faster (**Fig. 1c**). These 'complex maturation' kinetics were not caused by multimerization, since introducing the monomeric substitution A206K to wtGFP (mwtGFP) resulted in the same maturation curve (**Supplementary Fig. 6**). Similar complex maturation has previously been observed in red FPs[9–11]; however, several FPs derived from *Aequorea victoria* FPs (avFPs)—for example, moxGFP, SCFP1, mTurquoise2 and mClover3—also showed complex maturation kinetics, which indicated that such kinetics are not an exclusive property of red FPs. In view of this diversity of maturation kinetics, we chose to report two effective maturation times, t_{50} and t_{90}, that correspond to the time it takes for 50% or 90% of fluorescent proteins, respectively, to become mature (**Table 1** and **Supplementary Data 1**). Although the precise mechanism behind different maturation kinetics is unclear, we speculate that amino acids flanking the chromophore forming residues may play a key role (**Supplementary Fig. 7**).

The coding sequence (CDS) of FPs is often optimized with synonymous codons to increase FP expression in different organisms. Another common modification to improve expression is the addition of valine at the second amino acid position. We found that maturation kinetics were not affected by either change (**Supplementary Figs. 8** and **9**). By contrast, we discovered that many FPs reported in the literature under the same name had different nonsynonymous CDSs. The most surprising case was that of 'Venus', for which we found four slightly different

FAS Center for Systems Biology, Department of Molecular and Cellular Biology, School of Engineering and Applied Sciences, Harvard University, Cambridge, Massachusetts, USA. Correspondence should be addressed to P.C. (cluzel@mcb.harvard.edu).

RECEIVED 30 MARCH; ACCEPTED 20 OCTOBER; PUBLISHED ONLINE 20 NOVEMBER 2017; DOI:10.1038/NMETH.4509

nonsynonymous CDSs that we named VenNB[12], VenJBC[13], VenME[14], and VenSX[15], each of which had different maturation times. In such cases, we classified each nonsynonymous variant as a distinct FP.

There are several FPs that share the same β-barrel structure but have a different chromophore or different residues surrounding the chromophore. These FPs had different maturation times: the pattern was observed for the green FPs mEGFP, mGFPmut2 and mwtGFP; the blue FPs SCFP1, SCFP3A and mTurquoise2; and the yellow FPs mVenNB, VenJBC and mVenElo. For contrast, we decided to study the effect of specific mutations that would not perturb the chromophore environment. We selected four amino acid substitutions classified as 'spectroscopically silent' because they do not affect the spectroscopic properties of the chromophore: F99S[16], K206A (the revertant of the monomeric substitution A206K)[17], ΔC9 (truncation of the last nine C-terminal amino acids)[18], and ΔC9 combined with M153T[16]. These mutations were introduced into mGFPmut2. In all cases, the spectroscopically silent mutants retained maturation kinetics similar to those of mGFPmut2 (**Supplementary Fig. 10a–d**). Moreover, t_{50} and t_{90} were practically identical (**Supplementary Fig. 10e**,**f**), and the substitutions did not change the original mGFPmut2 spectra (**Supplementary Fig. 10g**). These experiments suggest that spectroscopically silent mutations do not necessarily affect maturation kinetics. Moreover, since mutations F99S and M153T have been associated with improved folding[16], these results suggest that chromophore maturation and folding are not intrinsically coupled processes.

Our experiments also revealed that the *in vitro* brightness of FPs ($F_{in\ vitro}$ = molar extinction (ε) × quantum yield (QY)) alone was a poor predictor of fluorescence signal in growing cells even when adjusted for differences in net expression levels ($F_{expression}$) (**Fig. 1d** and **Supplementary Data 2** and **3**). In turn, we hypothesized that by taking the maturation time into account as well, we could better predict fluorescence signal in growing cells. Indeed, we found that simply multiplying the term $F_{in\ vitro} \times F_{expression}$ with an additional factor that quantifies the interplay between maturation time (t_{50}) and dilution of proteins due to cell growth (t_{gr}), $F_{mat} = 1/(1 + t_{50}/t_{gr})$[19], was sufficient to robustly predict fluorescence signal in growing cells (**Fig. 1e**). A similar agreement was found between fluorescence signal in batch cultures quantified by flow cytometry and the product $F_{in\ vitro} \times F_{expression} \times F_{mat}$ (**Supplementary Fig. 11** and **Supplementary Data 4**). Note that in growing cell cultures, when FP expression is at steady state, fluorescence signal from fast FPs can be greater than that from slower FPs with similar or even greater *in vitro* brightness. We also found that variations in quantitation of *in vitro* brightness did not play a role as important as that of maturation time for selecting FPs with the greatest fluorescence signal in fast-growing cells (**Supplementary Fig. 12**).

We also investigated the effect of maturation time when FPs were used to report transcription in single cells. Under these conditions, FP expression can be highly dynamic and may not reach a steady state. For example, transcription from the *lacZ* promoter, P_{lacZ}, under repressed conditions (*lacI*$^+$ strain, glucose + no inducer) occurs in bursts[20]. To examine how maturation time would affect the measurement of such processes, we monitored the activity of the repressed P_{lacZ} driving the expression of either mGFPmut2 (fast) or mEGFP (slow). To ensure equal $F_{expression}$, both FPs had nucleotide sequences that were identical except for three residues unique to each FP. We also confirmed equal $F_{expression}$ by quantifying protein expression by SDS–PAGE gel densitometry (**Supplementary Fig. 13**). While both proteins had approximately the same *in vitro* brightness (ε × QY = 45.5 for mEGFP versus ε × QY = 39.3 for mGFPmut2), the signal from cells with mGFPmut2 was systematically stronger (**Fig. 2a**,**b** and **Supplementary Fig. 14**). Moreover, we observed richer promoter dynamics with the fast-maturing FP (**Fig. 2a**). We reasoned that, since fast FPs concentrate fluorescence signal within a shorter time window, they are better suited not only for temporal precision, but also for detecting small transient events (**Fig. 2c**). In line with this hypothesis, transcriptional bursts reported with the fast FP were consistently greater in amplitude than those reported with the slow FP (**Fig. 2d**). Moreover, the slow FP smeared the promoter dynamics so much that it almost resembled that of a constitutive promoter, a result which was in stark contrast to the previously reported burst activity of the repressed P_{lacZ}[20]. Overall, the dynamic range of the promoter

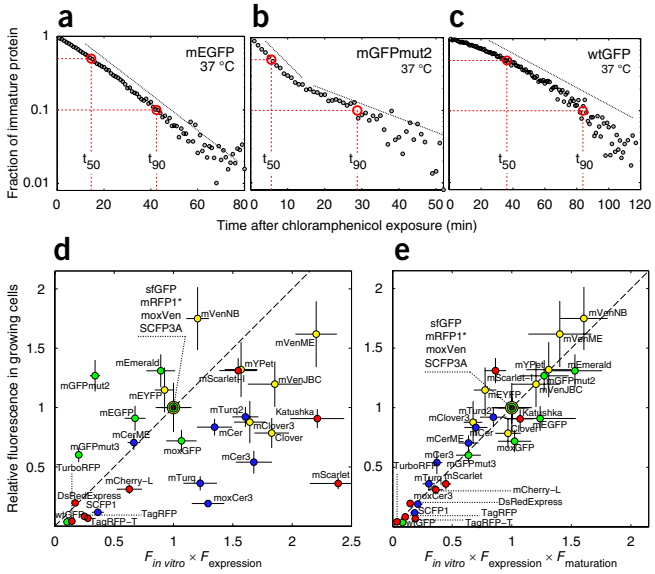

Figure 1 | Maturation kinetics and their impact on fluorescence signal in growing cells. (**a**–**c**) Fraction of immature protein as a function of time after translational arrest with chloramphenicol in single cells. (**a**) mEGFP maturation kinetics show a single exponential decay (dashed line). (**b**) mGFPmut2 exhibits a more complex maturation process with two kinetic steps (dashed lines). (**c**) wtGFP matures with a slow nonexponential rate that increases with time. Dashed red lines indicate the time it takes for 50%, t_{50}, and 90%, t_{90}, of FP to mature. (**d**) Fluorescence signal in growing cells versus $F_{in\ vitro}$ (= QY × ε) multiplied by $F_{expression}$ (= amount of protein). Fluorescence signal is the mean fluorescence of single cells (exponential growth in single-cell chemostat, M9-rich media, 37 °C, mean from 70 ± 20 cells, ±s.e.m.). For green FPs, data normalized by sfGFP data; for yellow FPs, by moxVenus data; for blue FPs, by SCFP3A data; and for red FPs, by mRFP1*. Dotted line is the identity. Dilution is given by the doubling time of *E. coli*, t_{gr} = 28.5 ± 2 min. (**e**) Fluorescence signal in growing cells versus $F_{in\ vitro} \times F_{expression}$ multiplied by $F_{mat} = 1/(1 + t_{50}/t_{gr})$[19]. Fluorescence signal data is the same as in **d**. QY and ε were quantified in our laboratory independently, except for *in vitro* data of red FPs (see Online Methods). We have assumed that the *in vitro* brightness of mRFP1* and mCherry-L is the same as the *in vitro* brightness of mRFP1 and mCherry, respectively, because amino acid differences are not part of the β-barrel. Error bars calculated by propagation of QY, ε and t_{50} errors.

Table 1 | Maturation time of common fluorescent proteins

FPs[a]	37 °C[b]		32 °C[b]	
	t_{50} (min)	t_{90} (min)	t_{50} (min)	t_{90} (min)
Cyan				
mCerulean	6.6 ± 0.5	24.0 ± 2.9	11.3 ± 0.9	50.7 ± 13.1
SCFP1	50.9 ± 2.8	118.5 ± 10.8	81[c]	189[c]
SCFP3A	6.4 ± 0.5	24.2 ± 2.7	10.6 ± 0.7	49.0 ± 15.3
mCerluean ME	7.4 ± 0.5	26.9 ± 2.2	12.1 ± 0.9	64.6 ± 13.7
mTurquoise	112.2 ± 7.1	319.9 ± 36.6	179[c]	512[c]
mCerulean3	69.8 ± 3.9	177.8 ± 17.8	112[c]	284[c]
mTurquoise2	33.5 ± 2.2	95.1 ± 9.3	58.7 ± 4.1	175.7 ± 21.7
moxCerulean3	100.4 ± 5.2	236.9 ± 23.6	159[c]	369[c]
Green (UV excitable)				
Sapphire	38.4 ± 2.4	103.4 ± 8.4	61[c]	165[c]
T-Sapphire	156.5 ± 11.2	478.2 ± 57.2	250[c]	765[c]
Green				
wtGFP	36.1 ± 2.1	83.8 ± 4.9	58[c]	134[c]
mEGFP	14.5 ± 1.0	42.4 ± 4.4	22.3 ± 1.5	62.8 ± 6.6
mGFPmut2	5.6 ± 0.4	28.8 ± 4.5	6.8 ± 0.5	20.0 ± 2.1
mGFPmut3[d]	4.1 ± 0.3	15.8 ± 3.1	4.5 ± 0.3	16.6 ± 2.9
mEmerald	11.2 ± 0.8	37.5 ± 12.1	17.7 ± 1.1	48.4 ± 4.0
sfGFP	13.6 ± 0.9	39.1 ± 4.7	19.4 ± 1.3	56.7 ± 6.0
moxGFP	17.1 ± 1.1	50.7 ± 4.3	35.7 ± 2.2	102.8 ± 17.4
Yellow-green				
mEYFP	9.0 ± 0.7	30.9 ± 4.2	10.6 ± 0.8	34.0 ± 4.3
mVenus NB	4.1 ± 0.3	18.4 ± 6.8	4.7 ± 0.4	18.0 ± 3.2
mVenus JBC	17.6 ± 1.3	59.1 ± 6.9	23.1 ± 1.7	87.1 ± 12.9
mYPet	9.7 ± 0.7	33.5 ± 5.4	11.9 ± 0.8	37.6 ± 4.3
mVenus ME	9.6 ± 0.7	30.9 ± 2.5	11.6 ± 0.8	37.9 ± 5.9
Venus SX	18.6 ± 1.3	57.7 ± 5.2	24.9 ± 1.8	74.4 ± 8.1
Clover	22.2 ± 1.4	61.6 ± 6.8	34.1 ± 2.2	108.3 ± 11.3
mNeonGreen	10.9 ± 0.8	36.8 ± 9.2	13.3 ± 0.9	37.7 ± 4.0
moxVenus	25.8 ± 1.8	77.8 ± 9.1	36.2 ± 2.7	119.0 ± 13.8
mClover3	43.5 ± 2.9	112.4 ± 9.6	63.5 ± 3.6	176.5 ± 19.8
Orange-red				
DsRed-Express	26.1 ± 1.4	70.8 ± 7.4	31.2 ± 1.1	85.8 ± 29.7
TurboRFP	87.8 ± 5.3	276.9 ± 33.5	142[c]	453[c]
TagRFP	42.1 ± 2.6	102.8 ± 7.8	51.9 ± 3.6	105.0 ± 6.4
TagRFP-T	42.4 ± 2.1	103.2 ± 6.0	55.1 ± 3.0	113.6 ± 6.0
DsRed-Expresss2	33.6 ± 1.8	78.5 ± 6.5	54[c]	126[c]
Red				
mRFP1	21.9 ± 1.1	51.4 ± 4.0	35[c]	82[c]
mRFP1*	23.8 ± 1.2	53.8 ± 4.7	32.5 ± 1.8	79.2 ± 9.1
mCherry-L	37.0 ± 1.8	81.4 ± 6.0	45.9 ± 3.4	105.7 ± 9.5
mCherry2-l	22.8 ± 1.2	51.3 ± 4.1	33.4 ± 2.1	83.1 ± 6.0
mRuby3	130.8 ± 6.8	342.4 ± 37.8	243.7 ± 15	725.0 ± 85.9
mRuby3 Addgene	136.5 ± 6.9	354.4 ± 39.0	243.7[c]	725.0[c]
mScarlet	132.4 ± 7.5	376.2 ± 43.4	212[c]	602[c]
mScarlet-I	25.7 ± 1.5	66.3 ± 6.8	32.8 ± 1.8	83.2 ± 8.8
Far red				
Katushka	34.0 ± 2.3	92.8 ± 8.4	55.9 ± 4.0	154.2 ± 13.8
mKate2	34.4 ± 1.8	79.4 ± 4.7	47.9 ± 2.8	113.8 ± 6.5
E2Crimson	23.4 ± 1.2	56.4 ± 4.9	30.8 ± 1.8	79.0 ± 9.5
Katushka9-5	27.4 ± 1.7	76.4 ± 7.2	44.5 ± 2.7	114.3 ± 15.4
mNeptune2	591.5 ± 44.8	1,982 ± 243	946[c]	3,171[c]
mNeptune2.5	34.5 ± 1.8	87.4 ± 6.9	82.0 ± 5.4	233.1 ± 26.9

[a]See **Supplementary Note** for a detailed description of the coding sequences and the references in which the FPs were initially described. [b]Because the kinetics in many cases does not follow a single exponential, we report two maturation times, t_{50} and t_{90}, ± confidence interval of 95%. Temperature has an error of ± 0.5 °C. [c]Estimated value of the maturation time at 32 °C was taken as 60% longer than the time measured at 37 °C; see Online Methods. For mRuby3 Addgene the estimated time at 32 °C is taken equal to that of mRuby3 at 32 °C. [d]Even though mGFPmut3 is the fastest maturing FP in the green category, its low photostability makes it a poor choice for time-lapse microscopy. **Supplementary Data 1** contains the mean fluorescence curves used to calculate maturation times.

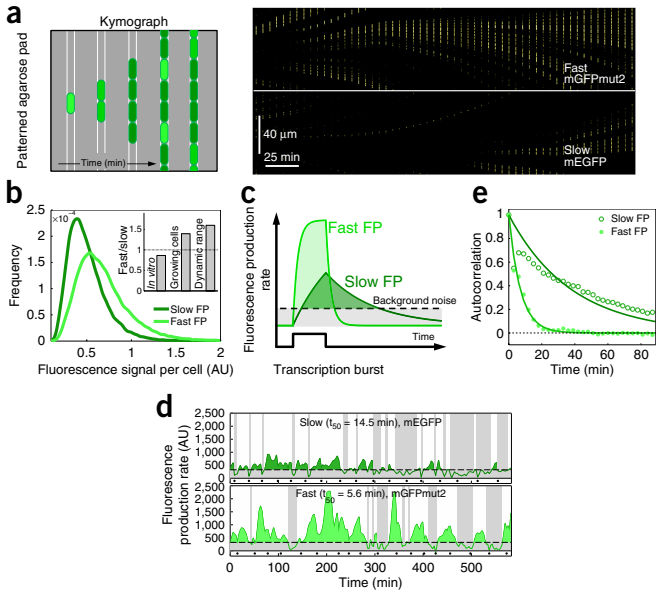

Figure 2 | Impact of maturation time on transcription dynamics. In growing cells, fluorescence signal associated with fast-maturing FPs can exhibit greater intensity and dynamic range than equally bright slow-maturing FPs. (**a**) Left, cartoon of a kymograph of a linear colony. Kymograph generated from the fluorescence channel of the time-lapse movie. Cells express stochastic bursts of an FP; intensity decreases because of dilution due to growth, thus creating the dark and bright bands in the kymograph. Right, kymograph made from the fluorescence channel showing that a fast FP reports brighter transcriptional events than a slower FP, even when both fluorophores have the same *in vitro* brightness. Upper half, fast FP (mGFPmut2, $\varepsilon \times QY = 39.3$, $t_{50} = 5.6$ min); lower half, slow FP (mEGFP, $\varepsilon \times QY = 45.5$, $t_{50} = 14.5$ min); expression driven by the repressed P_{lacZ} promoter. (**b**) Distribution of fluorescence signal per cell for the fast (light green, $n_{cell} = 2{,}489$) and the slow FP (dark green, $n_{cell} = 2{,}310$). Signal from the fast FP is always higher than that from the slow FP (**Supplementary Fig. 14**). Inset, *in vitro* brightness ratio, fluorescence-signal ratio in growing cells, and dynamic-range ratio between the fast and the slow FPs (**Supplementary Fig. 15**). (**c**) Black solid line, transcriptional burst that yields the same amount of either fast- or slow-maturing FPs. Black dashed line, hypothetical measurement limit set by background noise. (**d**) Time traces of the fluorescence production rate of the repressed P_{lacZ} using the fast or the slow FP. The detection limit (dashed line) is 3σ units above autofluorescence production rate; black dots indicate cell division, $t_{div} = 33$ min at 37 °C. Shaded bands indicate periods of promoter activity below the detection limit. (**e**) Autocorrelation of fluorescence production rate for the slow and the fast FP variants (characteristic decay times $t_{slowFP} = 24.5$ min and $t_{fastFP} = 6.3$ min). Both FPs are driven by the same promoter; thus, using the fast FP increases temporal resolution.

activity was 1.6 times greater when using the fast FP than when using the slow FP (**Supplementary Fig. 15**). Also, the fast FP could report faster promoter dynamics than the slow FP could (**Fig. 2e**). Based on the superior performance of the fast green FP, we predicted that the fastest cyan FP SCFP3A would be a better reporter than the brighter *in vitro*—but slower—mTurquoise2 ($\varepsilon \times QY = 28.7$ for mTurquoise2 versus $\varepsilon \times QY = 17.1$ for SCFP3A) to quantify the dynamics of the repressed P_{lacZ}. Indeed, the dimmer SCFP3A exhibited a 40% larger dynamic range and had three times better temporal resolution than the brighter *in vitro* mTurquoise2 (**Supplementary Fig. 16**) despite having similar expression levels (**Supplementary Fig. 13**).

Our work demonstrates that in growing cells, there exists a fraction of immature FPs, and that accounting for this fraction via the maturation time is crucial for explaining the relationship between *in vitro* brightness and fluorescence signal in growing cells (**Fig. 1e**). We hypothesize that, even in different environments, fast FPs will remain faster than slow FPs and thus remain preferable. For example, at different temperatures (37 °C and 32 °C), the ranking of maturation times is preserved; fast-maturing FPs still mature faster despite changes in the absolute maturation time. We note that independent of $F_{in\ vitro}$ and F_{mat}, fluorescence in growing cells may also unexpectedly vary because of organism-specific effects on net protein expression ($F_{expression}$) (extended discussion in **Supplementary Note**). However, as a general guide, we recommend the use of fast-maturing FPs, which will likely yield higher fluorescence signals—particularly in fast-growing cells—and, independent of growth rate, increase the temporal resolution of any time-lapse measurements. Specifically, our results show that SCFP3A, mGFPmut2 and mVenNB are likely the best fluorescent proteins to use for monitoring rapid cellular processes and that they will also give the brightest overall signal for monitoring rapid processes among the cyan, green and yellow classes, respectively. For the orange-red to far-red categories, we suggest avoiding slow-maturing red FPs and to be aware of their oligomeric tendency and the incomplete maturation of their chromophore, which sometimes gives rise to unintended emission in the blue-yellow part of the spectrum. In light of these limitations, we recommend mScarlet-I and mCherry2.

METHODS

Methods, including statements of data availability and any associated accession codes and references, are available in the online version of the paper.

Note: Any Supplementary Information and Source Data files are available in the online version of the paper.

ACKNOWLEDGMENTS

Thanks to A. Mendoza-García for help with spectroscopy, V. Pham for help with SDS-PAGE, P.J. Choi for the tsr-venus sequence, and J. Paulsson for useful comments. This work was partially supported by a fellowship from CONACYT-México and from the PEW Latin American Fellows Program to E.B.; a, NSF GRFP fellowship and Harvard University Ashford Fellowship to J.M.K. This work was supported by NSF 1615487, 1410176, DARPA HR0011-16-2-0049, and NIH 1R21AI094363.

AUTHOR CONTRIBUTIONS

E.B. and P.C. conceived the project and analyzed the data. E.B. performed cloning, biochemistry, single-cell experiments and software design for single-cell analysis. J.M.K. assisted with cloning and single-cell experiments. E.B. and J.M.K. designed software for time-lapse microscopy. E.B. and P.C. wrote the manuscript with critical revisions by J.M.K. P.C. supervised the project.

COMPETING FINANCIAL INTERESTS

The authors declare no competing financial interests.

1. Tsien, R.Y. *Annu. Rev. Biochem.* **67**, 509–544 (1998).
2. Shaner, N.C., Steinbach, P.A. & Tsien, R.Y. *Nat. Methods* **2**, 905–909 (2005).
3. Shaner, N.C., Patterson, G.H. & Davidson, M.W. *J. Cell Sci.* **120**, 4247–4260 (2007).

4. Day, R.N. & Davidson, M.W. *Chem. Soc. Rev.* **38**, 2887–2921 (2009).
5. Hebisch, E., Knebel, J., Landsberg, J., Frey, E. & Leisner, M. *PLoS One* **8**, e75991 (2013).
6. Megerle, J.A., Fritz, G., Gerland, U., Jung, K. & Rädler, J.O. *Biophys. J.* **95**, 2103–2115 (2008).
7. Craggs, T.D. *Chem. Soc. Rev.* **38**, 2865–2875 (2009).
8. Moffitt, J.R., Lee, J.B. & Cluzel, P. *Lab Chip* **12**, 1487–1494 (2012).
9. Bevis, B.J. & Glick, B.S. *Nat. Biotechnol.* **20**, 83–87 (2002).
10. Verkhusha, V.V. *et al. J. Biol. Chem.* **276**, 29621–29624 (2001).
11. Gross, L.A., Baird, G.S., Hoffman, R.C., Baldridge, K.K. & Tsien, R.Y. *Proc. Natl. Acad. Sci. USA* **97**, 11990–11995 (2000).
12. Nagai, T. *et al. Nat. Biotechnol.* **20**, 87–90 (2002).
13. Rekas, A., Alattia, J.R., Nagai, T., Miyawaki, A. & Ikura, M. *J. Biol. Chem.* **277**, 50573–50578 (2002).
14. Cox, R.S. 3rd, Dunlop, M.J. & Elowitz, M.B. *J. Biol. Eng.* **4**, 10 (2010).
15. Choi, P.J., Cai, L., Frieda, K. & Xie, X.S. *Science* **322**, 442–446 (2008).
16. Crameri, A., Whitehorn, E.A., Tate, E. & Stemmer, W.P. *Nat. Biotechnol.* **14**, 315–319 (1996).
17. Zacharias, D.A., Violin, J.D., Newton, A.C. & Tsien, R.Y. *Science* **296**, 913–916 (2002).
18. Kim, H.K. & Kaang, B.K. *Brain Res. Bull.* **47**, 35–41 (1998).
19. Wang, S., Moffitt, J.R., Dempsey, G.T., Xie, X.S. & Zhuang, X. *Proc. Natl. Acad. Sci. USA* **111**, 8452–8457 (2014).
20. Yu, J., Xiao, J., Ren, X., Lao, K. & Xie, X.S. *Science* **311**, 1600–1603 (2006).

ONLINE METHODS

Molecular cloning. All experiments and cloning were performed with *Escherichia coli* MG1655 (The Coli Genetic Stock Center, Yale University; CGSC 6300). All avGFP derivatives were constructed from an initial mGFPmut2 template used to generate linear fragments of dsDNA with the appropriate point mutations at the 5′ and 3′ ends. Linear fragments (from one to six fragments, depending on the FP) and the backbone were assembled together in a single isothermal assembly reaction[21]. The backbone confers kanamycin resistance and harbors the low-copy origin SC101. FP expression was controlled by a member of a set of constitutive promoters, *proC*[22], the T7 RBS and the T1 terminator. The mNeonGreen gene was a gift from J. Paulsson (Department of Systems Biology, HMS, Harvard University). All red FP genes were ordered as gBlocks from Integrated DNA Technologies (IDT) and cloned into a similar backbone as the one used for avGFPs. All FP coding sequences were confirmed by Sanger DNA sequencing from two clones. See **Supplementary Note** for the coding sequence definition of all FPs.

P_{lacZ} reporters with FPs of interest were cloned into the chromosome using the λ-Red homologous recombination system[23]. FPs were controlled by an RBS designed by Ishida and Oshima[24]. The RBS is a strong RBS and leaves the lacI binding site O1 and its context intact (**Supplementary Fig. 17**). There is a kanamycin cassette as selection marker located downstream of the FP gene. The sequences used as homologies for the integration were 5′AATTGTGAGCGGATAACAATTTCACACAGGAAACAGCTATGACCA and 5′TTAAATAGTACATAATGGATTTCCTTACGCGAAATACGGGCAGACATGGC.

Estimation of FP expression using SDS–PAGE gel densitometry. Exponentially growing cells were harvested at OD_{600} = 0.6, concentrated 15×, aliquoted and immediately stored at −80 °C for later processing. Later, 8 µl of thawed cells were mixed with 7 µl of 4× SDS–PAGE loading buffer and incubated at 98 °C for 12 min. Samples were loaded into a 4–20% SDS-PAGE gel. The gel was run at 200 V for 65 min. After electrophoresis, the gel was stained with Brilliant Blue and destained until the gel was transparent. The gel was imaged while taking special care not to overexpose the image. Densitometry analysis was performed with the software GelAnalyzer 2010a. Total protein density profile was background corrected using the rolling ball method. Using the protein profile from background strain MG1655, density contribution from endogenous proteins at ~27 kDa was estimated and subtracted from the raw FP value. FP densities were normalized using two sets of stereotypical total-protein bands around 40 kDa and 100 kDa. We ran two technical replicates with two different loading patterns to compensate for systematic gel distortions (**Supplementary Fig. 18**).

Protein extraction and purification. The three phase partitioning (TPP) procedure[25,26] was used to extract and purify avFPs. Cultures were grown from single colonies in 50 ml of LB Lennox with shaking at 30 °C for 2 d. Cells were pelleted down at 10,000 × *g* for 1 min and resuspended in 25 ml of 1.6 M ammonium sulfate in Tris–HCl buffer (50 mM Tris, pH 8.0). The resuspension was shaken for 30 min, and cells were again pelleted at 10,000 × *g* for 10 min and resuspended in 7.5 ml of 1.6 M ammonium sulfate.

1st stage of three phase partitioning. A 2.4 ml aliquot from the resuspension was transferred to a 5 ml Eppendorf tube and mixed vigorously for 10 min at 37 °C in a vortex mixer with a special adaptor to fit 5 ml tubes. Subsequently, 2.6 ml of t-Butanol was added, and the mixture was again shaken vigorously for 10 min at 37 °C. The 5 ml tube was centrifuged at 21,000 × *g* for 5 min to separate the mixture into three phases. The bottom phase (~2 ml) was transferred into a fresh 5 ml Eppendorf tube by piercing through the upper two layers and aspirating.

2nd stage of TPP. 3 ml of t-Butanol was added to the recovered phase, and the mixture was shaken vigorously for 5 min at 37 °C and centrifuged at 21,000 × *g* for 10 min to separate the mixture into three phases, the second phase being an extremely thin disc with all the FP. The thin disc was separated by slowly decanting the bottom and upper phases; the thin FP disc remained stuck to the wall of the tube. The tube was left standing for 1 min, and the residual t-Butanol/ammonium sulfate at the bottom was aspirated. The FP disc was redissolved in 150–250 µl of 1.6 M ammonium sulfate.

3rd stage of TPP. The 5 ml tube with the redissolved FP was centrifuged at 21,000 × *g* for 20 min. The crystal-clear aqueous phase was transferred with a pipettor to a sterile 1.5 ml Eppendorf tube. Care was taken to avoid pelleted debris and to avoid aspirating possible residual t-Butanol (a thin upper layer). Purified protein was stored at 4 °C.

Spectroscopy. Fluorescence spectra were acquired in a Horiba/Yvon FluoroMax-4 Spectrofluorometer. The instrument corrects for excitation lamp fluctuations and compensates for the spectral dependence of detector efficiency. Spectra were acquired with a 1 nm resolution, and the mean spectrum was derived from four readings using the following parameters: YFP Ex 482 and Em 497-685, GFP Ex 455 Em 470-675 and Cyan Ex 425 Em 445-750. The integration range for CFPs was broad enough to capture the complete tail of the coumarin reference dye. Samples were at least a 20× dilution (in Tris-HCl buffer, pH 8) of the purified protein recovered at the end of the 3rd stage of the TPP. Thus, final ammonium sulfate concentration was at most 70 mM.

Absorbance spectra were acquired using a Shimadzu SolidSpec-3700/3700DUV. To avoid reabsorption effects, samples and standard dyes were diluted until the absorption maximum did not exceed a reading of 0.1 units. Three spectrum readings were taken and averaged. We used polymethyl methacrylate (PMMA) cuvettes, BrandTech Scientific 759125. Cuvettes were taken from the same box (i.e., same mold cavity for all cuvettes, manufacturer description) to ensure lowest variation in extinction coefficient. In comparison to the absorption maxima of FPs, the extinction-coefficient variation due to cuvette manufacturing was less than 0.5%. Thus, all the FP spectra were corrected with the same average background absorption for a given box of cuvettes (**Supplementary Fig. 19**).

Estimate of quantum yield and molar extinction coefficient. SDS–PAGE densitometry was used to estimate the amount of purified FP at the end of the 3rd step of TPP. Briefly, 3.25 µl of purified protein in 1.6 M ammonium sulfate was mixed with 5.75 µl of 4× SDS–PAGE sample-loading buffer in PCR tubes. FP samples were denatured by heating at 98 °C for 12 min. In parallel, a dilution series of purified BSA (concentrations: 1.000, 0.666,

doi:10.1038/nmeth.4509

0.500, 0.333, 0.250, 0.167, 0.125, 0.083, 0.062, 0.041, 0.031 µg/µl) was prepared. FP samples were spiked with 8 µl of BSA standard such that every sample would have a different known BSA concentration. Volume was adjusted to 20 µl. Samples were loaded into a 4–20% SDS–PAGE gel. After electrophoresis, the gel was stained with Brilliant Blue and destained until the gel was transparent. The gel was imaged while taking special care not to overexpose the image. Image was analyzed with the Gel Analysis plug-in from ImageJ[27]. A standard curve using the known concentrations and corresponding band densities obtained from the Gel Analysis plug-in was created in Matlab R2013a (**Supplementary Fig. 20**). The standard curve was used to estimate the total amount of FP loaded in every well. The molar concentration of the sample was obtained assuming the weight of the FP as 26.89 kD. The molar extinction was determined using Beer's law.

We performed a relative determination of fluorescence quantum yields (QYs)[28],

$$\mathrm{QY}_{f,x} = \mathrm{QY}_{f,\mathrm{st}} \frac{F_x\, f_{\mathrm{st}}\, n_x^2(\lambda_{\mathrm{em}})}{F_{\mathrm{st}}\, f_x\, n_{\mathrm{st}}^2(\lambda_{\mathrm{em}})}$$

where F is the integral photon flux, f the absorption factor at the excitation wavelength ($f = 1 - 10^{-\mathrm{Abs}(\lambda \mathrm{ex})}$) and n the refractive index. st denotes the dye reference and x the FP sample. The refractive indexes of three solvents were needed to calculate $\mathrm{QY}_{f,x}$: ethanol 200 proof, 0.1 M NaOH and 50 mM Tris–HCl pH 8.0. Ethanol was the solvent for coumarin. For ethanol, the refractive index used was 1.364 (using the exact refractive index at the average coumarin emission gives negligible differences, http://refractiveindex.info). For 50 mM Tris–HCl pH 8, its refractive index was measured with a Milton Roy Abbe 3L refractometer with different amounts of dissolved ammonium sulfate. Results showed that the refractive index of Tris–HCl at relevant ammonium sulfate concentrations (<70 mM, after doing at least a 20× dilution from our stock of purified FP in ammonium sulfate 1.6 M) was equal to that of water at 25 °C, $n = 1.335$ at 500 nm, http://refractiveindex.info. The refractive index of 0.1 M sodium hydroxide, the fluorescein solvent, was also found to be equal to that of water. Note that, because the refractive index of water and ethanol are different, the refractive index ratio

$$\frac{n_x^2(\lambda_{\mathrm{em}})}{n_{\mathrm{st}}^2(\lambda_{\mathrm{em}})}$$

reduces the relative QY of blue FPs by about 4%. The reference dyes were fluorescein 'reference standard' (Molecular Probes F-1300, Lot# 1691-3) and coumarin 153 (99% purity, Sigma-Aldrich 546186-100MG, lot# MKBV7586V). The QYs used were 0.89 and 0.53, respectively[28]. For every FP, the protein was extracted/purified, the molar concentration determined and the absorbance/emission spectrum acquired from three independent cultures. QY and molar extinctions were determined from those three independent extractions for all FPs except for moxCerulean, mEmerald, moxGFP, moxVenus. For these FPs, only two independent extractions were performed. Reported errors are s.d.

Estimation of maturation time by translational arrest with chloramphenicol. *Single-cell chemostat assembly.* Briefly[8], polydimethylsiloxane (PDMS) chambers were cast using homemade metal molds. Then, chambers and glass coverslips were treated with O_2 plasma (Harrick Plasma; 18 W, 25 s, 1,000 mTor atmosphere) and put into contact to induce covalent bonding between the two surfaces. Subsequently, the chamber was pierced at its ends to create an inlet and an outlet with 30G needles. To avoid leakages, needles were sealed to PDMS chambers with a drop of freshly prepared PDMS and left to cure for 2 h at 55 °C. Meanwhile, a patterned agarose slab was prepared by pouring dissolved low-melt agarose (BP165, Fisher Scientific) on top of a PDMS intermediate that had on its surface the negative pattern to be printed on the agarose. Then, the PDMS chamber and a second square coverslip were plasma treated (as above). Immediately after, 2 µl of saturated cell culture ($OD_{600} \approx 1$) was dispensed at the center of the PDMS chamber, the patterned agarose slab was pressed into place, and the chamber was sealed with the square coverslip. The assembled single-cell chemostat was allowed to set for 15–30 min before intubating to introduce growth media.

Growth media composition. M9-rich media: M9 salts 1×, casamino acids 0.1%, glucose 0.5%, thiamine 1 µg/ml, $MgSO_4$ 2 mM, $CaCl_2$ 0.1 mM. The day before the experiment, growth media was prepared, its pH was checked (7.1 ± 0.2), and liquid cultures of individual colonies were set for overnight growth. The next morning, cells were diluted 200× in fresh media and incubated for 3–4 h before they were loaded into the single-cell chemostat. For the P_{lacZ} experiment, the same M9-rich media composition was used, except that the amount of casamino acids was reduced 200-fold to decrease background fluorescence (final concentration 0.005%). The decrease in nutrients increased division time by ~5 min.

Temperature calibration. Single-cell chemostat temperature at the objective was carefully characterized for different buffer flow rates (**Supplementary Note**). 4 h before starting a maturation experiment, the microscopy setup was left to equilibrate to the desired temperature.

Buffer exchange. The output of two 30 ml syringes (one with growth media, the other one with growth media plus chloramphenicol 100 µg/ml) were connected together to a two-input valve with stopcock (Value Plastics). The valve output was connected to the single-cell chemostat. To ensure exponential growth rate before data acquisition, cells were grown inside the chemostat for 4 h at 37 °C with growth media flowing at a rate of 50 µl/min via a peristaltic pump (KDS-210, KD Scientific). Then, data were acquired for 1 h at a rate of one frame per minute. After the first hour, the first pump was stopped, and the second pump, with growth media and chloramphenicol, was activated at a rate of 70 µl/min. At this rate, growth media in the single-cell chemostat was exchanged in <20 s with media with chloramphenicol. After buffer exchange and without interruption, data were acquired for another 3–4 h. Because of cell wall damage induced by chloramphenicol treatment, there is an artifactual dependence of photobleaching on chloramphenicol concentration. Nonetheless, there is a chloramphenicol concentration range (40–200 µg/ml) where photobleaching rate is constant (**Supplementary Note** and **Supplementary Fig. 21**).

Microscopy. Time lapses were taken with a Zeiss Axiovert 200M and a Plan-Apochromat 40×/1.3 Oil Ph3. Focal-plane drift was eliminated by using software-based autofocus following the method described in ref. 29. In short, we characterized the frequency response of our optical system (camera/objective)

to filter out low- and mid-range frequencies from *Z*-stacks. Those frequencies are responsible for unwanted contrast reversals usually found in regular software-based autofocuses. A solid-state white illumination SOLA SE II was used for fluorescence excitation. The filter set for the green channel was Ex. 482/18, Di. 495, Em. 520/35; for the yellow channel it was Ex. 500/24, Di. 520, Em. 542/27; for the blue channel it was Ex. 438/24, Di. 458, Em. 483/32; and for the red channel it was Ex. 586/20, Di. 605, Em. 647/57; all filters were from Semrock. Images were acquired with a CCD camera (Hamamatsu C4742-98-24ERG). Variation in fluorescence intensity illumination across the field of view was less than 10% in all channels. Under our experimental conditions, most maturation curves do not exhibit measurable photobleaching; see **Supplementary Note** and **Supplementary Figures 22** and **23**. The microscope setup was controlled with homemade software using Micro-Manager 1.4 (ref. 30) and Matlab R2013a.

Calculation of the immature fluorescent protein fraction from single-cell data. *Selection of single cells*. Kymographs of individual linear colonies were constructed from time-lapse movies that contained a phase contrast and a fluorescence channel. Using the phase-contrast kymographs, we backtracked—starting from the last frame—only cells that remained in the tracks of the agar pad and that did not lyse.

Single-cell fluorescence quantification. For every single cell, using the fluorescence channel kymograph, raw fluorescence was quantified at frame *t* by adding signal from all pixels within a rectangular window that was twice the width of the cell in order to capture all out-of-focus light (**Supplementary Fig. 24**). To measure the background fluorescence as a function of time, a kymograph of an agar pad strip without cells was constructed. To obtain a background-corrected fluorescence value at frame *t*, the background quantified from the empty agar pad strip at frame *t* was subtracted from the raw fluorescence value at frame *t*.

Averaging of data. Independently of colony membership, to obtain a mean fluorescence curve, fluorescence data from all cells were added and divided by the number of cells. Similarly, but with single-cell-length data, a mean-length curve was obtained. The mean-length curve was used to determine the precise moment at which chloramphenicol arrived.

Fraction of immature fluorescent protein. To obtain the fraction of immature protein, the mean fluorescence was subtracted from the maximum fluorescence value and divided by the fluorescence increase after drug treatment; see **Supplementary Figure 5** for a step-by-step diagram. All analysis was done using Matlab R2013a.

Fluorescence signal estimation by flow cytometry. Three replicate cultures for every avFP were grown overnight in M9-rich media at 37 °C. The next day, a first set of replicates was diluted 1,000× in fresh M9-rich media and incubated at 37 °C. After 20 min, the same procedure was followed for the second set of replicates and, finally, after an additional 20 min the third set was also diluted and incubated. The delay between replicates was set to minimize maturation time artifacts in the *in vivo* brightness determination using flow cytometry. Typically, a single set of replicates would take ~6 min to be quantified. After 2 h and 40 min from the first dilution, a second 500× dilution was performed for every set of replicates following the same time delay. After 2 h, the replicates were growing exponentially (OD_{600} = 0.05–0.1). An aliquot of the first set was transferred to a 96-well plate prewarmed to 37 °C and stored in a Styrofoam box. Immediately, samples were measured in a BD LSR Fortessa. The same was done for the second and the third bioreplicate sets. The excitation/emission configuration was CFP Ex. 440 (laser), Em. 470/20; GFP Ex. 488 (laser), Em. 520/35; and YFP Ex. 488 (laser), Em. 542/27.

Statistical methods. Immature FP fraction curves were initially obtained for several FPs (mEGFP, mGFPmut2, mGFPmut3, sfGFP, SCFP3A, mVenME, mCherry) with at least three independent replicates. Once the results from these initial FPs were reproducible, new FPs were measured together with a previously characterized FP as a control. If the control displayed an anomalous maturation curve, the experiment was not further analyzed. In a successful experiment, after ~2 h of chloramphenicol treatment, a small fraction of cells would lose their fluorescence, presumably because of cell wall damage (**Supplementary Note**). We manually eliminated these cells from the analysis. Mean single-cell fluorescence curves were derived from the mean of 70 ± 20 cells. We obtained the t_{50} and t_{90} values by smoothing the log-transformed immature FP fraction curves using the function csaps in MATLAB R2013a with a smoothing parameter equal to 0.01. Errors in quantifying maturation times were estimated by assuming the errors in the average fluorescence to be ±3%. The typical error in our average fluorescence curves is below 1% at fluorescence saturation. Thus, the assumed ±3% error in average fluorescence gives at least a confidence interval of 66% (1 s.d.) and typically a confidence interval of 95% (2 s.d.). For specific FPs, the maturation time at 32 °C was estimated using the maturation time measured at 37 °C (**Supplementary Fig. 25**). QY and ε average and s.d. were derived from three independent protein extractions except for moxCerulean, mEmerald, moxGFP, moxVenus. For these FPs, only two independent extractions were performed. QY and ε values used for the *x*-axis of **Figure 1d** are the values reported when the FPs were first published, except for mVenusME and mCeruleanME; for these two FPs, we used our own *in vitro* data (**Supplementary Tables 1** and **2**). In the *x*-axis of **Figure 1e**, the red FP *in vitro* data were taken from different laboratories (**Supplementary Table 2** and **Supplementary Fig. 26**). For all other FPs, QY and ε were quantified in our laboratory (**Supplementary Table 1**). We estimated FP expression by SDS densitometry. $F_{expression}$ is the median ± s.d. of four measurements from two SDS gels (**Supplementary Figs. 13** and **18**; **Supplementary Data 2**). The two gels were technical replicates. Errors of derived experimental quantities (e.g., $F_{in\ vitro}$ error) were obtained by propagation of errors from values experimentally determined (e.g., quantum yields and extinction coefficients). In time traces, single-cell-fluorescence production rate was approximated by finite differences and the result smoothed with the function filtfilt using a filter order equal to 3 and a cutoff frequency equal to 0.55 (Matlab R2013a). Autocorrelation of fluorescence production rate was calculated along cell lineages, and sampling bias was eliminated by avoiding counting branches more than once[31]. The estimated autocorrelation decay constants were obtained by fitting the theoretical autocorrelation function given in ref. 20. We repeated a single experiment with FPs of different colors: two greens (mGFPmut2 and mEGFP) and two blues (SCFP3A and mTurquoise2) to support the robustness of the observed effect in **Figure 2**.

doi:10.1038/nmeth.4509

Code availability. Code to generate **Figure 2** and **Supplementary Figure 16** can be found in Dataverse at doi:10.7910/DVN/THTGHS. Code to analyze single-cell data from the single-cell chemostat experiments is available from the corresponding author upon request.

Life Sciences Reporting Summary. Further information on experimental design and reagents is available in the **Life Sciences Reporting Summary**.

Data availability. Fluorescence maturation curves, SDS–PAGE gel densitometry calculations, a worksheet to obtain **Figures 1** and **2** and SDS–PAGE images of FP-expressing *E. coli* total lysate are available with the paper online. Data to obtain **Figure 2** and **Supplementary Figure 16** can be found in Dataverse: doi:10.7910/DVN/YH7LHM and doi:10.7910/DVN/OVZMXF. Flow cytometry source data of **Supplementary Figure 11** can be found in Dataverse: doi:10.7910/DVN/T4VSGH. Maturation-time experiments from which **Table 1** and **Figure 1** were derived can be found in Dataverse: doi:10.7910/DVN/KBNK6R. FPs listed in **Table 1**, codon-optimized FPs and 2nd valine FPs are available at Addgene, IDs from 103968 to 103991 and from 103993 to 104033. A detailed step-by-step protocol is accessible as a **Supplementary Protocol**.

21. Gibson, D.G. *et al. Nat. Methods* **6**, 343–345 (2009).
22. Davis, J.H., Rubin, A.J. & Sauer, R.T. *Nucleic Acids Res.* **39**, 1131–1141 (2011).
23. Yu, D. *et al. Proc. Natl. Acad. Sci. USA* **97**, 5978–5983 (2000).
24. Ishida, M. & Oshima, T. *J. Biochem.* **132**, 63–70 (2002).
25. Thomson, C.M. & Ward, W.W. Three-phase partitioning (TPP): a rapid and preparative purification tool for GFP. in. *Bioluminescence and Chemiluminescence, Progress & Current Applications* (eds. Stanley, P.E. & Kricka, L.J.) 115–118 (World Scientific, 2002).
26. Ward, W. In *Protein Purification* (Ed. Rizwan Ahmad) Ch. 1 (InTech, 2012).
27. Schneider, C.A., Rasband, W.S. & Eliceiri, K.W. *Nat. Methods* **9**, 671–675 (2012).
28. Würth, C., Grabolle, M., Pauli, J., Spieles, M. & Resch-Genger, U. *Nat. Protoc.* **8**, 1535–1550 (2013).
29. Oliva, M.A., Bravo-Zanoguera, M. & Price, J.H. *Appl. Opt.* **38**, 638–646 (1999).
30. Edelstein, A.D. *et al. J. Biol. Methods* **1**, e10 (2014).
31. Dunlop, M.J., Cox, R.S. 3rd, Levine, J.H., Murray, R.M. & Elowitz, M.B. *Nat. Genet.* **40**, 1493–1498 (2008).

nature research

Corresponding author(s): Philippe Cluzel

☐ Initial submission ☐ Revised version ☒ Final submission

Life Sciences Reporting Summary

Nature Research wishes to improve the reproducibility of the work that we publish. This form is intended for publication with all accepted life science papers and provides structure for consistency and transparency in reporting. Every life science submission will use this form; some list items might not apply to an individual manuscript, but all fields must be completed for clarity.

For further information on the points included in this form, see Reporting Life Sciences Research. For further information on Nature Research policies, including our data availability policy, see Authors & Referees and the Editorial Policy Checklist.

Experimental design

1. Sample size

Describe how sample size was determined.

Fig 1a-c. Sample size was not pre-determined. See Table 1 below.

Fig 1d. Y-axis. Sample size was not pre-determined. The mean was derived from 75 +/-20 cells. The error is the SEM and is on average 20%. X-axis. Net protein expression was derived from two replicates for each FP. This is enough to distinguish 20% changes in net protein expression. Compared to the range of relative fluorescence signal covered by our FP library (see range of X- and Y-axis in Fig 1d), data errors in the X- and Y-axis are almost 10 times lower and, as quantified by the r-squared, allows us to clearly distinguish the effect of maturation time between Fig. 1d and Fig. 1e.

Fig 1e. Y-axis. Same as Fig 1d. Y-axis. X-axis. Sample size was not predetermined. Quantum yield and molar extinction were derived from 3 protein extractions. This is enough to distinguish 15% changes in in vitro brightness. Net protein expression was derived from two replicates for each fluorescent protein. This is enough to distinguish 20% changes in net protein expression. The t50 maturation time error is below 10%. Propagating the previous errors results in about a 20% error in the estimated relative fluorescence. This error is almost 10 times lower than the range of relative fluorescence signal covered by our FP library in Fig 1d-e and, as quantified by the r-squared, allows us to clearly distinguish the effect of maturation time between Fig. 1d and Fig. 1e.

Fig. 2b, Fig. 2e, S Fig. 15 and S Fig. 16. Sample size was not pre-determined. mGFPmut2, ncell=2489, mEGFP, ncell= 2581, mTurquoise2 ncells=1460 and SCFP3A ncells=1711. Fig.2b. Sample size is large enough that fluctuations in the tail of the distribution are only seen after the 99th percentile. Fig. 2e and S Fig. 16b. The sampling of the autocorrelation functions diminishes as the lag time increases. However, the sampling was high enough at lag time 80min in Fig. 2e (n=12000) and at lag time 150min (n=7500) in Fig. 16b to ignore fluctuations. S Fig. 15 and S Fig. 16c. Sample size was enough to have a robust estimation of the dynamic range, i.e. the dynamic range ratio (fast FP)/(slow FP) is similar using the 1st and the 99th percentile, or using the 2nd and the 98th percentile.

Table 1. Sample size was not pre-determined. Maturation curves were calculated from 75+/-20 cells. At 25% and at 100% fluorescence, the experimental fluctuation of maturation curves (local CV value) is, for the great majority, well below 3% and 1%, respectively. Because the trend of the maturation curve (obtained by a smoothing filter) is robust to experimental fluctuations, we derived reliable t50 and t90 values from all curves and reported 95% confidence intervals.
To see fine details of the maturation kinetics at, e.g. 90% fluorescence, error needs to be lower than 1:10. As mentioned above, our error around 100% fluorescence saturation is below 1:100. Thus, for almost all curves, fluctuations around the mean trend are very low and allow to see the fine details of the maturation kinetics. Exceptions are, at 100% fluorescence, DsRedEx 32°C (4.9%), TagRFP 32°C (3.1%), TagRFP-T 32°C (4.7%).

Nature Methods: doi:10.1038/nmeth.4509

2. Data exclusions

Describe any data exclusions.

Fig. 1 and Table 1. A few cells would anomalously lose fluorescence after ~2hrs of chloramphenicol treatment due, presumably, to cell-wall damage. We plotted the single-cell fluorescence vs time of all tracked cells to visually detect and eliminate those cells from the analysis. Cells were eliminated because including them would have created artificial photobleaching and thus would have altered maturation kinetics measurements.

Fig. 2 and S Fig. 16. An experiment in the single-cell chemostat is recorded using many fields of view (FOV). Some FOVs are not analyzable because (i) local fluorescence background is too high due to bad buffer flow, (ii) or cells do not grow along the linear tracks and create biofilms instead of linear colonies or (iii) the microscope software would fail to track the FOV. We only included in the analysis, linear colonies from FOV without these problems.

3. Replication

Describe whether the experimental findings were reliably reproduced.

Fig. 1 and Table 1. Immature FP fraction curves were initially obtained for several FPs (mEGFP, mGFPmut2, mGFPmut3, sfGFP, SCFP3A, mVenME) with at least 3 independent replicates. Once the results from these initial FPs were reproducible, new FPs were measured together with a previously characterized FP as a control. If the control displayed an anomalous maturation curve, the experiment was not further analyzed.

Fig. 2 and S Fig. 16. We performed a single experiment with FPs of different colors: two greens (mGFPmut2 & mEGFP) and two blues (SCFP3A & mTurquoise2) to support the robustness of the observed effect.

4. Randomization

Describe how samples/organisms/participants were allocated into experimental groups.

It does not apply to our work because we do not have different experimental groups, e.g. a treatment and a control group.

5. Blinding

Describe whether the investigators were blinded to group allocation during data collection and/or analysis.

Blinding is not relevant to our study because we knew the identity of every measured FP.

Note: all studies involving animals and/or human research participants must disclose whether blinding and randomization were used.

6. Statistical parameters

For all figures and tables that use statistical methods, confirm that the following items are present in relevant figure legends (or in the Methods section if additional space is needed).

n/a	Confirmed
☐	☒ The exact sample size (*n*) for each experimental group/condition, given as a discrete number and unit of measurement (animals, litters, cultures, etc.)
☐	☒ A description of how samples were collected, noting whether measurements were taken from distinct samples or whether the same sample was measured repeatedly
☐	☒ A statement indicating how many times each experiment was replicated
☒	☐ The statistical test(s) used and whether they are one- or two-sided (note: only common tests should be described solely by name; more complex techniques should be described in the Methods section)
☒	☐ A description of any assumptions or corrections, such as an adjustment for multiple comparisons
☒	☐ The test results (e.g. *P* values) given as exact values whenever possible and with confidence intervals noted
☐	☒ A clear description of statistics including central tendency (e.g. median, mean) and variation (e.g. standard deviation, interquartile range)
☐	☒ Clearly defined error bars

See the web collection on statistics for biologists for further resources and guidance.

Software

Policy information about availability of computer code

7. Software

Describe the software used to analyze the data in this

We used custom software to obtain, from time lapses, kymographs of linear

Nature Methods: doi:10.1038/nmeth.4509

study.

colonies and to track and quantify the fluorescence of cells. The software is available upon request. All software was written in Matlab R2013a.

For manuscripts utilizing custom algorithms or software that are central to the paper but not yet described in the published literature, software must be made available to editors and reviewers upon request. We strongly encourage code deposition in a community repository (e.g. GitHub). *Nature Methods* guidance for providing algorithms and software for publication provides further information on this topic.

Materials and reagents

Policy information about availability of materials

8. Materials availability

Indicate whether there are restrictions on availability of unique materials or if these materials are only available for distribution by a for-profit company.

No unique materials were used.

9. Antibodies

Describe the antibodies used and how they were validated for use in the system under study (i.e. assay and species).

No antibodies were used.

10. Eukaryotic cell lines

a. State the source of each eukaryotic cell line used.

No eukaryotic cell lines were used.

b. Describe the method of cell line authentication used.

No eukaryotic cell lines were used.

c. Report whether the cell lines were tested for mycoplasma contamination.

No eukaryotic cell lines were used.

d. If any of the cell lines used are listed in the database of commonly misidentified cell lines maintained by ICLAC, provide a scientific rationale for their use.

No eukaryotic cell lines were used.

Animals and human research participants

Policy information about studies involving animals; when reporting animal research, follow the ARRIVE guidelines

11. Description of research animals

Provide details on animals and/or animal-derived materials used in the study.

The study did not involve research animals.

Policy information about studies involving human research participants

12. Description of human research participants

Describe the covariate-relevant population characteristics of the human research participants.

The study did not involve human research participants.

Nature Methods: doi:10.1038/nmeth.4509

nature research

Corresponding author(s): Philippe Cluzel

☐ Initial submission ☐ Revised version ☒ Final submission

Flow Cytometry Reporting Summary

Form fields will expand as needed. Please do not leave fields blank.

Data presentation

For all flow cytometry data, confirm that:

☒ 1. The axis labels state the marker and fluorochrome used (e.g. CD4-FITC).

☒ 2. The axis scales are clearly visible. Include numbers along axes only for bottom left plot of group (a 'group' is an analysis of identical markers).

☒ 3. All plots are contour plots with outliers or pseudocolor plots.

☒ 4. A numerical value for number of cells or percentage (with statistics) is provided.

Methodological details

5. Describe the sample preparation.	Three replicate cultures for every avFP were grown overnight in M9 rich media at 37°C. Next day, a first set of replicates was diluted 1000X in fresh M9 rich media and incubated at 37°C. After 20 min, the same procedure was followed for the second set of replicates and, finally, after an additional 20 more minutes the third set was also diluted and incubated. The delay between replicates was set to minimize maturation time artifacts in the in vivo brightness determination using flow cytometry. Typically, a single set of replicates would take ~6min to be quantified. After 2hrs 40min from the first dilution, a second 500x dilution was performed for every set of replicates following the same time delay. After 2hrs, the replicates were growing exponentially (OD600 = 0.05-0.1). An aliquot of the first set was transferred to a 96-well plate pre warmed to 37°C and stored in a styrofoam box. Immediately, samples were measured in a BD LSR Fortessa. The same was done for the second and the third bio-replicate sets.
6. Identify the instrument used for data collection.	Samples were measured in a BD LSR Fortessa. The excitation/emission configuration was CFP Ex 440 (laser), Em 470/20; GFP Ex 488 (laser), Em 520/35; and YFP Ex 488 (laser), Em 542/27.
7. Describe the software used to collect and analyze the flow cytometry data.	Flowing Software 2.5.1
8. Describe the abundance of the relevant cell populations within post-sort fractions.	Greater than 95%
9. Describe the gating strategy used.	For green FPs, cell-like objects were separated from a clear debris fraction by using the side and forward scattering. Then, cell objects were identified by gating only events with green fluorescence (FITC channel). The same was done for yellow FPs and cyan FPs. For the latter, the cyan channel was used in the second gaiting. We have exemplified the gating strategy in Supplementary Figure 11.

Tick this box to confirm that a figure exemplifying the gating strategy is provided in the Supplementary Information. ☒

Nature Methods: doi:10.1038/nmeth.4509